

Solvate Ionic Liquids for Li, Na, K, and Mg Batteries

Toshihiko Mandai,^[a] Kaoru Dokko,^{*[b, c]} and Masayoshi Watanabe^[b]

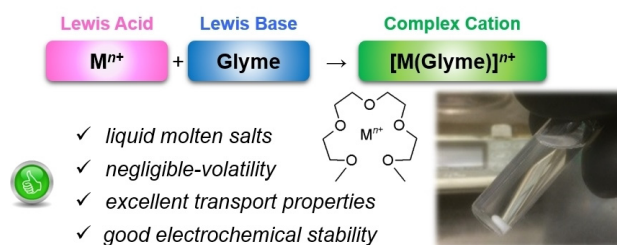
Abstract: From the viewpoint of element strategy, non-Li batteries with promising negative and positive electrodes have been widely studied to support a sustainable society. To develop non-Li batteries having high energy density, research on electrolyte materials is pivotal. Solvate ionic liquids (SILs) are an emerging class of electrolytes possessing somewhat superior properties for battery applications compared to conventional ionic liquid electrolytes. In this account, we describe our recent efforts regarding SIL-based electrolytes for Li, Na, K, and Mg batteries with respect to structural, physicochemical, and electrochemical characteristics. Systematic studies based on crystallography and Raman spectroscopy combined with thermal/electrochemical stability analysis showed that the balance of competitive cation–anion and cation–solvent interactions predominates the stability of the solvate cations. We also demonstrated battery applications of SILs as electrolytes for non-Li batteries, particularly for Na batteries.

Keywords: Batteries, Chelates, Electrochemistry, Ionic liquids, Sodium

1. Introduction.

Rapidly increasing demands for electric power sources require the parallel development of highly efficient energy-harvesting technologies. Li-ion batteries have responded to such demands, and indeed have offered fascinating advancements in a variety of portable devices, electric vehicles, and smart grid systems. The limited resources of Li, Co, and natural graphite, however, may hinder the use of Li batteries for large-scale applications.^[1,2] From the viewpoint of element strategy, post Li-ion batteries, particularly those incorporating cost-effective non-Li metals, such as Na, K, Ca, Mg, and Al, have been considered as promising candidates for large-scale electrochemical energy storage systems.^[1–16]

Because of safety concerns, electrolyte materials should possess sufficient thermal stability, particularly in large-scale battery applications as such batteries would require a great amount of chemically/electrochemically active materials to deliver/store electrical energies, thus simultaneously risking thermal runaway in accidents. Ionic liquid (IL)-based electrolytes can address many issues arising from the use of conventional organic liquid-based electrolytes owing to their remarkable thermal stability, negligible volatility, and non-flammability.^[17,18] Solvate ILs (SILs) are a newly emerging class of ILs and are defined as ILs consisting of solvate ions and their counter ions (Scheme 1).^[19,20] We have extensively



Scheme 1. Illustration of the concept of SILs.

[a] T. Mandai

Faculty of Science and Engineering, Iwate University
4-3-5 Ueda, Morioka, Iwate 020-8551, Japan

[b] K. Dokko, M. Watanabe

Department of Chemistry and Biotechnology, Yokohama National University,
79-5 Tokiwadai, Hodogaya-ku, Yokohama 240-8501, Japan

[c] K. Dokko

Unit of Elements Strategy Initiative for Catalysts & Batteries (ESICB),
Kyoto University, Kyoto 615-8510, Japan

investigated the fundamental structural aspects and characteristics for electrolyte applications. A representative SIL [Li(G3 or G4)][TFSA] (G3: triglyme, G4: tetraglyme, TFSA: $\text{N}(\text{SO}_2\text{CF}_3)_2^-$) exhibits similar properties to those of conventional onium-based ILs.^[20–29] Several researchers have also taken interest in the concentrated and/or equimolar glyme-Li salt systems.^[30–40] The comprehensive investigations based on both experiments and calculations have shown that the formation of stable solvate cations is responsible for the high thermal and enhanced electrochemical stabilities.^[20,23,28,41] SIL-based electrolytes have also shown excellent performance in various advanced Li-based batteries.^[29,42–46]

In addition to Li-based SILs, non-Li-based SILs also show sufficient high thermal stabilities, negligible volatility, and non-flammability with acceptable ionic conductivity.^[28,47–54] The electrochemical stabilities are also effectively enhanced upon complexation of glymes with metal ions. The high reductive and oxidative stabilities of non-Li-based SILs facilitate their usage as electrolytes for various prospective batteries. In this account, we present our recent efforts regarding the development of SILs consisting of Li, Na, K, and Mg salts with glymes, with respect to structural, physicochemical, and electrochemical characteristics. A combination of crystallography and vibrational analysis is particularly helpful in characterizing the structure of complexes in both crystalline and liquid states. The choice of metal ion (M^{n+}) was found to strongly affect not only the

structures but also the physicochemical properties and stabilities of the resulting complexes. The magnitude of stability enhancement is discussed based on the ionic nature of each metal species with the aid of quantum chemical calculations. We also propose the possibilities of SILs as electrolytes for next-generation battery applications, particularly for Na batteries. In this account, we mainly focus on the non-Li-based SILs. Regarding the detailed fundamental properties of Li-based SILs and their battery applications, the interested reader is directed to the recent review article.^[29]

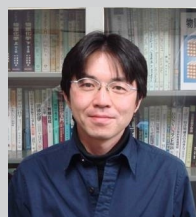
2. Structure and Properties of Na, K, and Mg-based SILs

2.1 Structural Aspects

Phase behavior and complexation: As well as the Li-based systems, certain binary mixtures of Na, K, and Mg salts and glymes (G_n , $\text{CH}_3\text{O}(\text{CH}_2\text{CH}_2\text{O})_n\text{CH}_3$) also form solvates at stoichiometric ratios, 1:1 and/or 1:2 for salt:glyme, irrespective of the choice of salts and glyme length.^[28,47,51,52,54] The phase diagrams of these mixtures indeed clearly illustrate features characteristic of complex formation. Maxima of melting point (T_m) are typically observed at a 1:1 molar ratio, implying that equimolar complexes are formed (Figure 1). For some limited cases, T_m maxima are observed only or additionally at a 1:2 molar ratio, as shown in Figures 1



Toshihiko Mandai received his Ph.D. degrees in 2012 under supervision of Prof. K. Nishikawa from Chiba University. He was a postdoctoral fellow at Yokohama National University with Prof. M. Watanabe, at Chalmers University of Technology with Prof. P. Johansson, and at Tokyo Metropolitan University with Prof. Kiyoshi Kanamura. In 2017, he was appointed as an assistant professor at Iwate University. His research interests include structure of ionic complexes and battery electrolytes.



Kaoru Dokko is a Professor of Yokohama National University. He received Ph.D from Tohoku University in 2001, and he did postdoctoral research at Case Western Reserve University and Tokyo Metropolitan University. He was appointed as an associate professor at Yokohama National University in 2008 and promoted to a full professor in 2016. His current research



interests are the physicochemical properties of concentrated electrolytes, nano-structured materials for energy conversion and storage, and electrochemical reaction process in electrochemical devices.

Masayoshi Watanabe is a Professor of Yokohama National University. He received his B.S., M.S., and Ph.D. degrees from Waseda University. He joined Sophia University in 1982 as an Assistant Professor. In 1992, he moved to Yokohama National University and was promoted to full Professor in 1998. He received the Award of the Society of Polymer Science, Japan in 2006, and the Award of The Electrochemical Society of Japan (Takei Award) and ECS Max Bredig Award in 2016. His current research interests include the design of ionic liquids and polymers for electrochemical applications and the phase-behavior and self-assembly of polymers in ionic liquids.

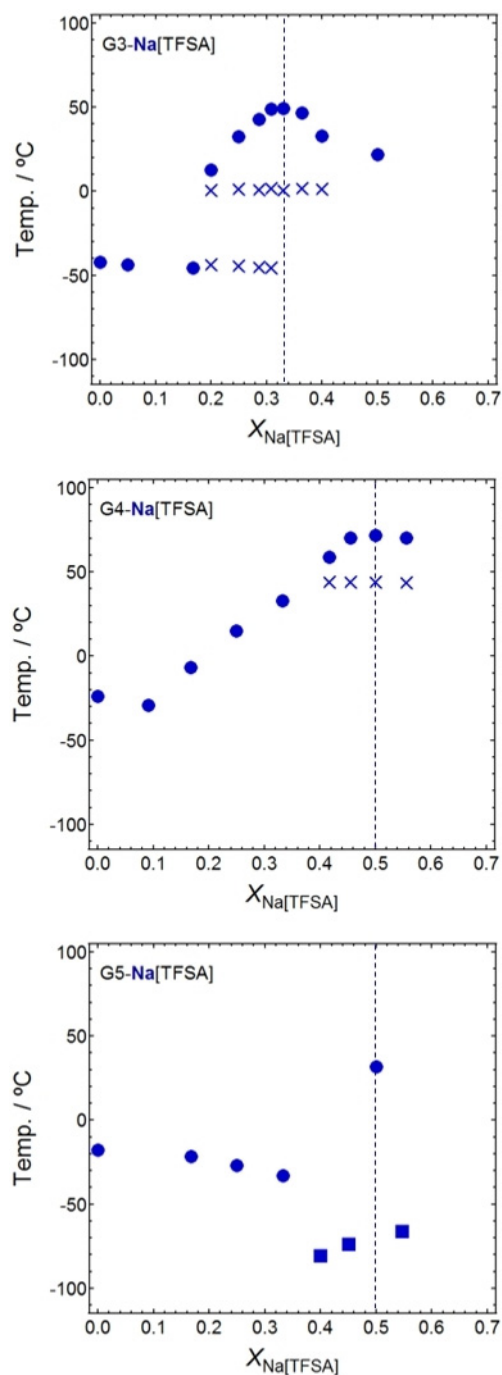


Figure 1. Typical example of phase diagrams of the G3-Na[TFSA] (upper), G4-Na[TFSA] (middle), and pentaglyme (G5)-Na[TFSA] (lower) systems as a function of the mole fraction of Na[TFSA]. Closed circles are melting points, closed squares are glass transition temperatures, and crosses are other thermal transition temperatures (not revealed). Reproduced from Ref. 28 with permission from the American Chemical Society.

and 2.^[28,54] This observation supports the formation of 1:2 complexes. The complexes that involve two equivalent glyme

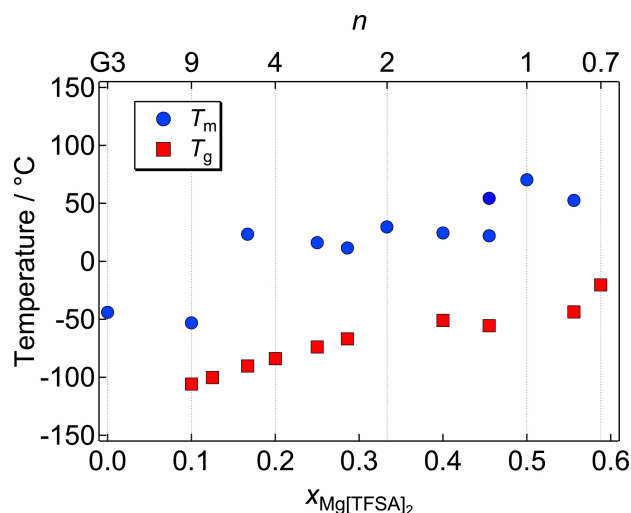


Figure 2. Phase diagram of Mg[TFSA]₂ and G3 binary mixtures with various salt mole fractions in the range of $x=0.10$ – 0.59 (molar ratio $n=9$ – 0.7 , where $G3/Mg[TFSA]_2=n$). Reproduced from Ref. 54 with permission from the PCCP Owner Societies.

molecules were also reported for the LiX–G2 (X: anion, G2: diglyme) systems.^[32,55] The stoichiometry of the complex formation is governed by the glyme length, metal ion radius, and preferential coordination number of the metal ion. A detailed discussion based on the coordination structure follows.

Thermogravimetric (TG) analysis on the binary mixtures of salts and glymes is also useful in evaluating whether binary mixtures form stoichiometric solvates. Figure 3 shows temperature-dependent and isothermal TG curves for the binary mixtures of Na[TFSA] and G4, as an example.^[47] As seen in Figure 3, the thermal stability of the mixture improves with salt concentration, and the equimolar complex [Na(G4)][TFSA] has a significantly high thermal stability. This result implies that complexation of metal ions with glymes inhibits evaporation owing to strong ion–solvent interactions while free (uncoordinated) glymes can easily evaporate even at a relatively low temperature. The three-step TG curves observed in the temperature-dependent TG curves clearly illustrate several thermal events occurring in the diluted ($n > 1$) systems. The same stepwise behavior of TG curves was observed for other salt-glyme combinations which form stoichiometric complexes. In particular, complexation of glymes with Mg[TFSA]₂ leads to a remarkable improvement in thermal stability, indicating exceptionally strong interaction between the Mg²⁺ and glymes (Figure 4).^[54] It should be noted that the thermal stability of 1:2 complexes is insufficient compared to the corresponding equimolar complexes.^[28,54] For example, [Na(G3)₂][FSA] (FSA: N(SO₂F)₂⁻) and [Al(G3)₂][Al(TfO)₄(OH)₂].G3 (TfO: CF₃SO₃⁻) easily

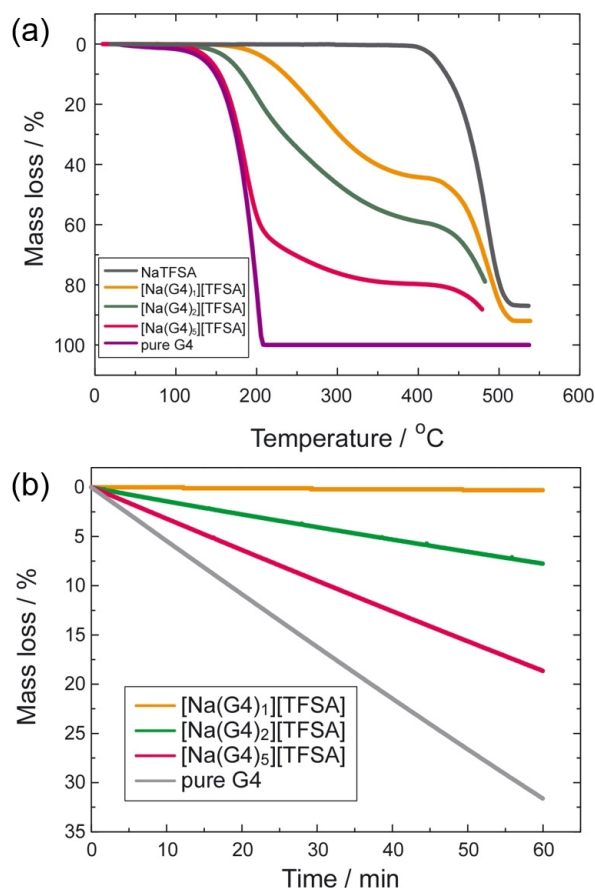


Figure 3. (a) Temperature-dependent and (b) isothermal TG curves of $[\text{Na}(\text{G}4)_n][\text{TFSA}]$ with pure G4 and $\text{Na}[\text{TFSA}]$. Isothermal stability was evaluated by monitoring the mass loss maintaining the temperature at 100°C . Reproduced from Ref. 47 with permission from the American Chemical Society.

release the coordinated glyme molecules in the molten state.^[56,57] The presence of uncoordinated glymes can be assessed via isothermal TG analysis, as shown in Figure 3b. The electrolytes containing excess glyme ($x > 1$ in $[\text{Na}(\text{G}4)_x][\text{TFSA}]$) lost weight with time because of the evaporation of uncoordinated glymes, while no mass loss was observed for the equimolar complex.

In addition to the salt–glyme ratio, the choice of cations and anions also has a significant impact on the stability of the resulting complexes. The equimolar complexes paired with strong Lewis basic anions are thermally less stable compared to those with weak Lewis basic anions.^[24,51] In the binary mixtures, there is competition between glymes and anions for interactions with a metal ion (M^+). Electrostatic (ion-dipole) and induction (ion-induced dipole) interactions between the cation and glyme largely contribute to the M^+ –glyme attraction.^[41,53] Of course, interactions between the cation (M^+) and anion occur, and the interionic interactions

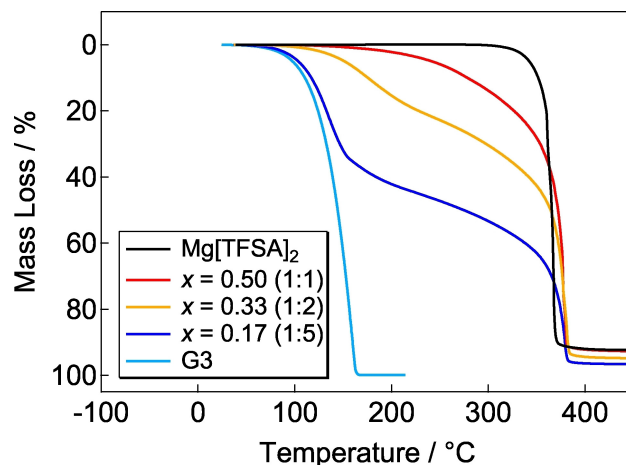


Figure 4. TG curves for $\text{Mg}[\text{TFSA}]_2$ and G3 binary mixtures with different $\text{Mg}[\text{TFSA}]_2$ concentrations together with the corresponding data for neat G3 and $\text{Mg}[\text{TFSA}]_2$. Reproduced from Ref. 54 with permission from the PCCP Owner Societies.

strengthen as the Lewis basicity of an anion strengthens.^[24] Therefore, an appropriate combination of glyme- M^+ -anion (salt-glyme) in which the M^+ –glyme interaction overwhelms the M^+ –anion interactions is very important to achieve structurally stable cation complexes.

Coordination structure in the crystalline states: We have reported the coordination structure of a series of metal-glyme solvates in the crystalline state.^[28,47,51–54] Henderson et al. have also extensively studied the phase behavior and crystal structures of many different solvates mainly incorporating Li salts.^[32–34] X-ray crystallography is among the most powerful and suitable tools to characterize the structures of solvates. The crystal structures of $[\text{M}(\text{glyme})][\text{TFSA}]_n$ ($\text{M} = \text{Li}, \text{Na}, \text{K}, \text{and Mg}$) are shown in Figure 5. Although the phase diagrams suggest the formation of $[\text{Na}(\text{G}3)]_2[\text{TFSA}]$, $[\text{K}(\text{G}4)]_2[\text{TFSA}]$, and $[\text{K}(\text{G}4)][\text{TFSA}]$ complexes, these structures could not be determined because of their low crystallinity. The crystal structure of an equimolar mixture of $\text{Li}[\text{TFSA}]$ and G4, $[\text{Li}(\text{G}4)][\text{TFSA}]$, has also not been clarified as this complex is strongly prone to the supercooling state. However, the crystal structures of the $[\text{Na}(\text{G}3)]\text{X}$, $[\text{Na}(\text{G}3)_2]\text{X}$, $[\text{K}(\text{G}4)_2]\text{X}$, and $[\text{Li}(\text{G}4)]\text{X}$ (X : anions other than $[\text{TFSA}]$) complexes have been reported elsewhere.^[34,38,51,56,58]

In the crystals, each metal ion is surrounded by a flexible glyme chain, and oxygen atoms in the structure all participate in coordination, thereby forming a $[\text{M}(\text{glyme})]^{n+}$ complex cation. The coordination shell formed in $[\text{M}(\text{glyme})]^{n+}$ complexes is coordination center dependent even though the same glyme is used. For example, pentaglyme (G5) coordinates to the K^+ ion to form a complex cation $[\text{K}(\text{G}5)]^+$ analogous to $[\text{K}(\text{18C}6)]^+$ (18C6: 18-crown-6 ether), whereas

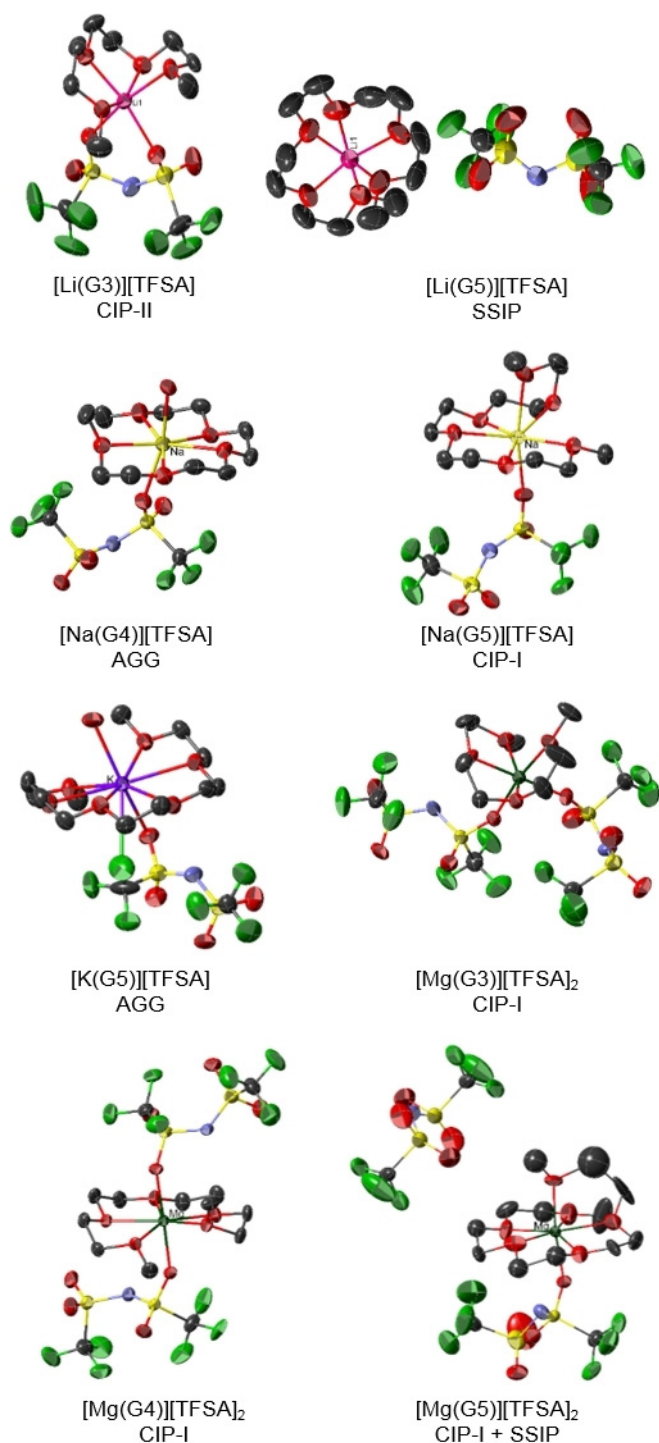


Figure 5. Crystal structures of $[M(\text{glyme})][\text{TFSA}]_n$ with the type of solvates defined by the coordination manner of the $[\text{TFSA}]^-$ ion: solvent-separated ion pair (SSIP); contact ion pair with a monodentate anion (CIP-I); contact ion pair with a bidentate anion (CIP-II); and aggregate, a single anion coordinated to two or more cations (AGG). The structures were created using each crystallographic information file (cif) deposited in the Cambridge Crystallographic Data Centre (CCDC). Thermal ellipsoids are drawn at a 50% probability level, and hydrogen atoms are omitted for clarity. Gray, C; red, O; light blue, N; light green, F; yellow, S; pink, Li; dark yellow, Na; purple, K; and dark green, Mg.

G5 and Li^+ or Na^+ ions form characteristic complex cations $[\text{Li}(\text{G5})]^+$ or $[\text{Na}(\text{G5})]^+$, as shown in Figure 5. A Li^+ ion within $[\text{Li}(\text{G5})]^+$ is tightly wrapped by a single G5 molecule forming a structure analogous to a helix $[\text{Li}(\text{PEO})]$ complex.^[39,59] However, a coordination structure similar to the $[\text{Na}(\text{15C5})]^+$ complex was found for $[\text{Na}(\text{G5})]^+$, and one excess oxygen atom perpendicularly coordinates to Na^+ . In addition, a single $[\text{TFSA}]^-$ ion participates in the coordination of Na^+ with a monodentate form. These differences arise from the preferential coordination structure and ionic radius of each metal ion. It is well known that the binding affinity between metal ions and crown-ether molecules strongly depends on their size; Li, Na, K, and Mg ions fit well with the 12C4, 15C5, 18C6, and 15C5 ethers, respectively. The flexible glyme chain allows for a configuration suitable for each metal ion, and glyme molecules coordinate to metal ions in a characteristic manner depending not only on glyme length but also the metal species. Note that highly distorted coordination of glymes was found for $[\text{Li}(\text{G3})][\text{TFSA}]$ and $[\text{Mg}(\text{G3})][\text{TFSA}]_2$. A slight mismatch in size is likely the reason for these observations.

The counter $[\text{TFSA}]^-$ ions also coordinate to metal ions in various forms, resulting in CIP-I-, CIP-II-, or AGG-type solvates depending on their composition (Figure 5), with the exception of $[\text{Li}(\text{G5})][\text{TFSA}]$. In the case of $[\text{Li}(\text{G5})][\text{TFSA}]$, an SSIP-type solvate, in which the $[\text{TFSA}]^-$ ion does not participate in the coordination with the Li^+ ion, is formed. For glyme- $M[\text{TFSA}]_n$ complexes, metal ions are preferentially coordinated by glyme.^[41] Hence, the preferential coordination number of each metal ion determines whether and how a $[\text{TFSA}]^-$ ion contributes to solvate formation.

The coordination manner of anions is slightly different for the complexes incorporating other than $[\text{TFSA}]^-$. The solvates with $[\text{TfO}]^-$ and ClO_4^- ions, such as $[\text{Na}(\text{G4})]\text{ClO}_4$ and $[\text{K}(\text{G5})][\text{TfO}]$, form CIP-type solvates (Figure 6), whereas the corresponding solvates with the $[\text{TFSA}]^-$ ion result in AGG-type solvates (Figure 5). These differences were also seen in the corresponding crown-ether-based complexes; $[\text{K}(\text{18 C6})][\text{TFSA}]$ is an AGG-type solvate while $[\text{K}(\text{18 C6})][\text{TfO}]$ is a CIP-II-type solvate.^[51] The cause of this phenomenon is considered to be related to the formation energy E_{form} of the parent salts. The complexes with the larger E_{form} of the parent salts tend to form CIP-type solvates, probably owing to the stronger M^+ -anion interaction compared to M^+ -glyme interaction. A somewhat curious solvate was found for the $[\text{Mg}(\text{G5})][\text{TfO}]_2$ solvate, in which five oxygen atoms within the G5 molecule coordinate to a single Mg^{2+} in a 15C5-like framework, and one remaining oxygen atom does not participate in coordination. Two $[\text{TfO}]^-$ ions further perpendicularly coordinate to Mg^{2+} in a monodentate form, thereby forming a sandwich-type CIP-I solvate. An exquisite balance of solvation power between G5

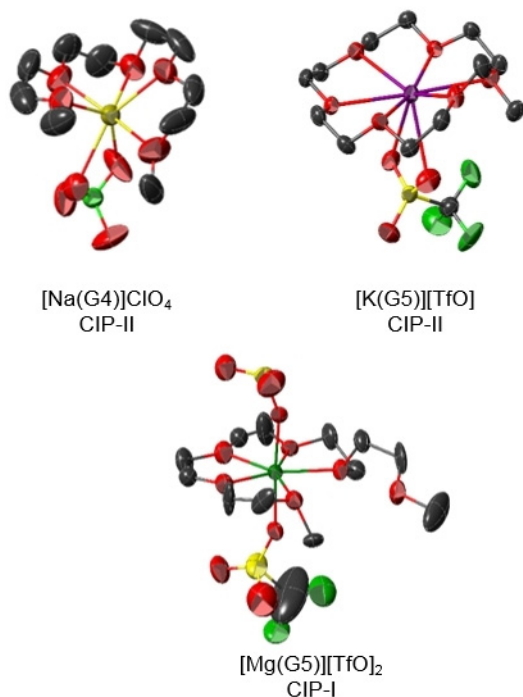


Figure 6. Crystal structures of $[\text{Na}(\text{G}4)]\text{ClO}_4$, $[\text{K}(\text{G}5)][\text{TfO}]$, and $[\text{Mg}(\text{G}5)][\text{TfO}]_2$. Because of the low crystallinity, the structure of $[\text{Mg}(\text{G}5)][\text{TfO}]_2$ could not be precisely determined. Thermal ellipsoid models of $[\text{Na}(\text{G}4)]\text{ClO}_4$ and $[\text{K}(\text{G}5)][\text{TfO}]$ were created using a crystallographic information file (cif) deposited in the Cambridge Crystallographic Data Centre (CCDC), while the structure of $[\text{Mg}(\text{G}5)][\text{TfO}]_2$ was derived from unreported experimental data. Thermal ellipsoids are drawn at the 50% probability level, and hydrogen atoms are omitted for clarity. Gray, C; red, O; light green, F; yellow, S; dark yellow, Na; purple, K; and dark green, Mg.

and $[\text{TfO}]^-$ ions for interaction with Mg^{2+} would lead to such a specific structure formation.

Coordination structure in the liquid state: The coordination structure of crystalline glyme-MX complexes can be determined precisely using X-ray crystallography. The complexation of glymes with metal ions in the molten/liquid states can be detected and qualified by analyzing the intra- and inter-molecular vibrational modes of the molten/liquid and crystalline states together with the corresponding crystal structures. A Raman active, characteristic vibrational mode was observed at ca. $870\text{--}890\text{ cm}^{-1}$ and readily assigned to a combination of CH_2 rocking, $\nu(\text{CH}_2)$, and CO stretching, $\nu(\text{CO})$, modes of glymes in the $[\text{M}(\text{glyme})]^{n+}$ cation, the so-called ring-breathing mode. As no bands for pure glymes were observed in the range $865\text{--}890\text{ cm}^{-1}$ while many different conformers were severely overlapping in the range $800\text{--}860\text{ cm}^{-1}$,^[60] this intense band is among the fingerprints of complex formation. The breathing mode is indeed evident in the crystalline $[\text{M}(\text{glyme})]\text{X}$ complexes. The solvates with multivalent metal ions lead to a blue shift of the breathing

mode,^[52,54,57] suggesting the position of the breathing mode is a useful indicator for interactions of glymes with metal ions.

Figure 7 shows typical examples of the Raman spectra for $[\text{Na}(\text{G}4)_n]\text{X}$ in the range $780\text{--}900\text{ cm}^{-1}$, adopted to the range for vibration of glymes, as a function of the glyme ratio to salts.^[47] The peak intensity at ca. 855 cm^{-1} , assignable to the

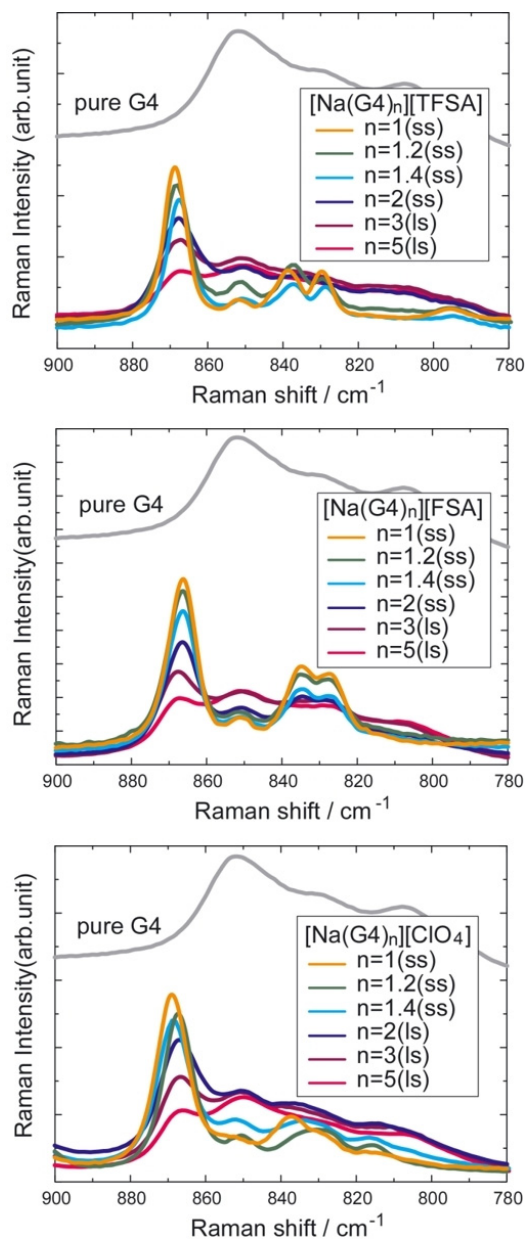


Figure 7. Concentration dependence of the Raman spectra in the range of $780\text{--}900\text{ cm}^{-1}$ for $[\text{Na}(\text{G}4)_n]\text{X}$ with $[\text{TFSA}]^-$ (upper), $[\text{FSA}]^-$ (middle), and ClO_4^- (lower) ions. Raman spectrum of pure G4 is also included in each figure. The captions “ss” and “ls” in each figure correspond to “solid state” and “liquid state”, respectively. Reproduced from Ref. 47 with permission from the American Chemical Society.

vibrational mode of pure glymes, gradually decreases with a decrease in the ratio of glymes to salts, and a sharp peak simultaneously emerges at ca 870 cm^{-1} . The equimolar mixture provided a completely different spectrum. The broad Raman bands assignable to non-coordinated glymes nearly vanished, implying that nearly all glymes coordinate to metal ions to form crown-ether-like solvates. The change in solution state, from diluted solution to SIL, can be clearly observed. The concentration-dependent thermal stability of the binary mixtures of salts and glymes can be explained with respect to the corresponding Raman spectra: the thermal stability of the binary mixtures improves upon consuming uncoordinated solvents. Similar results were also observed for the different salt and glyme combinations, except for the binary mixtures of NaX-G3, KX-G4, and $\text{MgX}_2\text{-G3}$.^[28,54] The latter three systems can form 1:2 complexes, as previously described. The 1:2 complexes obviously have a band at a different frequency from the band of 1:1 complexes. The concentration dependence of such binary systems showed characteristic behavior, particularly for the breathing mode.

Estimation and understanding of the coordination structure of the complexes in the molten state is extremely important for the electrolyte application because the coordination state of metal ions and the presence/absence of free glymes susceptibly affect the physicochemical properties and battery performance (*vide infra*). As characteristic Raman spectra are observed for the complexes, the variation in the spectra upon phase transition clearly demonstrates the solvate stability.

As previously stated, the stability of solvates (or lifetime of solvate cations) is salt-glyme combination dependent because the M^+ -anion interaction competes with the M^+ -glyme interaction. For glyme- $\text{M}[\text{TFSA}]$ systems, broad Raman peaks assignable to uncoordinated glymes emerge in the spectra of typical 1:2 complexes $[\text{M}(\text{glyme})_2][\text{TFSA}]$ through phase transition.^[28] This result indicates desolvation of glymes from their complex cation structures upon melting. Nevertheless, some crystalline solvates are successfully isolated; hence, they are thermodynamically stable in the crystalline state. In contrast, similar (cationic) spectra are observed for the other equimolar complexes irrespective of the phase states (solid or liquid) and choice of metal ions. These indicate that the 1:1 complexations between glymes and metal ions are favorable for achieving the high structural stability of the cationic complexes.

Quite drastic spectral variation can be observed for the equimolar complexes incorporating relatively strong Lewis basic anions. As previously mentioned, strong Lewis basic anions impart rather strong M^+ -anion interactions compared to M^+ -glyme interactions. The former interaction is likely to become more pronounced in the molten state probably because of the reorganization of components. Figure 8 shows

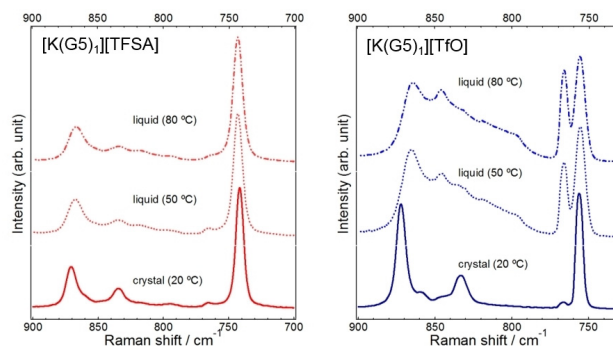


Figure 8. The effect of temperature on the Raman spectra of (left) $[\text{K}(\text{G5})][\text{TFSA}]$ and (right) $[\text{K}(\text{G5})][\text{TfO}]$. The spectra were measured at 20, 50, and $80\text{ }^\circ\text{C}$ using a hermetically sealed capillary to avoid absorbing any impurities. The phase states of each sample at recorded temperatures are described in the spectra. Reproduced from Ref. 51 with permission from the PCCP Owner Societies.

the Raman spectra of $[\text{K}(\text{G5})][\text{TFSA}]$ and $[\text{K}(\text{G5})][\text{TfO}]$ measured at different temperatures.^[51] Very minor spectral variation was found for the complexes with relatively weak Lewis basic anions $[\text{TFSA}]^-$. In contrast, the spectral shape considerably changed upon melting for the complex with the $[\text{TfO}]^-$ ion. As evidenced from this spectral variation, the Lewis basicity of the anions has a critical impact on the stability of the solvate cation. The effect of anion choice on the structures and stability of solvate cations have extensively been studied especially for Li-based SILs,^[24,27,32–34,38,39,61] and incorporation of weak Lewis basic amide-type anions is a very effective approach to create good SILs.^[20] The same approach is certainly applicable to Na, K and Mg-based SILs.

2.2 Stability of Solvate ILs

Glymes coordinated to metal ions are highly polarized owing to the strong electric field of the metal ions. The electrostatic ion–dipole and induction interactions contribute to the thermal and electrochemical stability of complexes. In this section, we discuss the thermal and electrochemical stabilities of the Na, K, and Mg-based SILs with the aid of quantum chemical calculations. Note that, because limited combinations of salts and glymes result in sufficiently stable solvates, the characteristics of SILs incorporating only amide anions are reported hereafter to maintain the focus.

Thermal stabilities: The thermal stability of glymes is significantly enhanced upon complexation with appropriate salts. The magnitude of the thermal stability enhancement, estimated from differences in the thermal decomposition temperatures (ΔT_{4s}) between the complexes and the corresponding pure glymes, is a good measure to clarify the effect of salts on thermal stability. Table 1 clearly indicates that complexation of glymes with metal ions strongly suppresses

the evaporation of the coordinated glymes. ΔT_d depends on the choice of glyme length and metal ion species. Particularly, the thermal stability of equimolar complexes is drastically improved by incorporating divalent Mg^{2+} ions. The magnitude of enhancement is nearly twice that of cases involving monovalent alkali metal ions.

As the parent salts would yield as an intermediate product through thermal degradation of $[\text{M}(\text{glyme})][\text{TFSA}]_n$ (*vide supra*), the desolvation energy of glymes from the $[\text{M}(\text{glyme})][\text{TFSA}]_n$ complexes (ΔE_{form}) should correlate with ΔT_d . ΔE_{form} can be calculated as the difference in the formation energies of the $[\text{M}(\text{glyme})][\text{TFSA}]_n$ and $\text{M}[\text{TFSA}]_n$ complexes. A strong relationship between ΔE_{form} and ΔT_d for $[\text{M}(\text{glyme})][\text{TFSA}]_n$ is indeed clearly observed (Tables 1 and 2). The ΔE_{form} values of the divalent $[\text{Mg}(\text{glyme})][\text{TFSA}]_2$ are considerably larger than those of the corresponding monovalent $[\text{M}(\text{glyme})][\text{TFSA}]_n$. Analysis of the interaction energies suggested that not only the electrostatic interaction but also the induction interaction between a metal ion and a glyme greatly contributes to the E_{form} for $[\text{M}(\text{glyme})][\text{TFSA}]_n$, in particular for $[\text{Mg}(\text{glyme})][\text{TFSA}]_2$.^[53] Taken altogether, remarkably strong electrostatic and induction interactions of divalent Mg^{2+} tightly attract both glymes and $[\text{TFSA}]^-$ ions, thereby forming exceptionally stable equimolar complexes.

Table 1. ΔT_d of a series of solvate ILs incorporating $[\text{TFSA}]^-$ ions. T_d of neat glymes are also included as a reference. The selected T_d data is extracted from Refs. 28, 52, and 54.

	$T_d/^\circ\text{C}$	$\Delta T_d/^\circ\text{C}$
neat G3	104	–
$[\text{Li}(\text{G3})][\text{TFSA}]$	190	86
$[\text{Mg}(\text{G3})][\text{TFSA}]_2$	241	137
neat G4	134	–
$[\text{Li}(\text{G4})][\text{TFSA}]$	205	71
$[\text{Na}(\text{G4})][\text{TFSA}]$	212	78
$[\text{Mg}(\text{G4})][\text{TFSA}]_2$	292	158
neat G5	176	–
$[\text{Li}(\text{G5})][\text{TFSA}]$	221	45
$[\text{Na}(\text{G5})][\text{TFSA}]$	234	58
$[\text{K}(\text{G5})][\text{TFSA}]$	220	44
$[\text{Mg}(\text{G5})][\text{TFSA}]_2$	318	142

Electrochemical stabilities: The strong electric field of small metal ions strongly polarizes the lone pairs of oxygen atoms of the coordinated glyme molecules, resulting in a lowering of their highest occupied molecular orbital (HOMO) energy levels. The HOMO energy level of anions is also influenced by the electric field effect of metal ions. As amide anions with highly delocalized charge distribution show remarkable stability toward oxidation (in general, > 5.0 V vs. Li/Li^+),^[62] electrochemical oxidation of SILs at the electrode|electrolyte interfaces is caused by the extraction

Table 2. Stabilization energies for $[\text{M}(\text{glyme})][\text{TFSA}]_n$ and $\text{M}[\text{TFSA}]_n$ complex formation. ΔE_{form} is the desolvation energy of glymes from the $[\text{M}(\text{glyme})][\text{TFSA}]_n$ complexes. The E_{form} and ΔE_{form} values are extracted from Refs. 28 and 53.

M, glyme	$E_{\text{form}}/\text{kcal mol}^{-1}$ $[\text{M}(\text{glyme})][\text{TFSA}]_n$	$\text{M}[\text{TFSA}]_n$	$\Delta E_{\text{form}}/\text{kcal mol}^{-1}$
Li, G3	–179.5	–137.2	42.3
Mg, G3	–536.5	–490.4	46.1
Li, G4	–181.3	–137.2	40.5
Na, G4	–152.1	–110.5	38.6
Mg, G4	–543.5	–490.4	53.1

of electrons from the HOMO of glymes. Therefore, lower HOMO energy levels of glymes impart a higher oxidative stability. The HOMO energy levels of glymes in the different environments, estimated using ab initio molecular orbital calculations, are summarized in Table 3. Variation in the HOMO energy levels of glymes upon complexation was also included as ΔHOMO .

Table 3. HOMO energy levels of glymes in the equimolar complexes with different coordination centers. The data is transcribed from Refs. 28, 52, and 53.

Samples	HOMO/eV	$\Delta\text{HOMO}/\text{eV}$
G3 (all trans)	–11.46	0
$[\text{Li}(\text{G3})][\text{TFSA}]$	–12.10	–0.64
$[\text{Mg}(\text{G3})][\text{TFSA}]_2$	–12.58	–1.12
G4 (all trans)	–11.46	0
$[\text{Li}(\text{G4})][\text{TFSA}]$	–11.83	–0.37
$[\text{Na}(\text{G4})][\text{TFSA}]$	–11.85	–0.39
$[\text{Mg}(\text{G4})][\text{TFSA}]_2$	–12.64	–1.18
G5 (all trans)	–11.46	0
$[\text{Li}(\text{G5})][\text{TFSA}]$	n.d.	n.d.
$[\text{Na}(\text{G5})][\text{TFSA}]$	–11.98	–0.52
$[\text{K}(\text{G5})][\text{TFSA}]$	–11.84	–0.38
$[\text{Mg}(\text{G5})][\text{TFSA}]_2$	n.d.	n.d.

As expected, the calculated HOMO energy levels of glymes in the equimolar complexes all lower upon complexation of metal ions. The magnitude of the reduction is, however, coordination center dependent. As well as the thermal stability enhancement, the valence of the coordination center has a significant impact on ΔHOMO . An exceptionally large reduction in the HOMO energy levels is observed for the complexes with divalent Mg^{2+} ions. The strong electric field of the Mg^{2+} ions strongly attract the lone pairs of ether oxygen atoms in the glymes, thereby drastically lowering the HOMO energy levels upon complexation with Mg^{2+} . However, no clear relationship between the size, i.e. charge density, of the metal ions and HOMO energy levels was found for the monovalent $[\text{M}(\text{glyme})][\text{TFSA}]$ complexes.

This is probably because of the models used in the calculation and the less noticeable difference in the electric field effect on the HOMO energy levels among the Li^+ , Na^+ , and K^+ ions.

To assess the change in the HOMO energy levels upon complexation, linear sweep voltammetry (LSV) was performed on a series of equimolar complexes. The LSV experiment was conducted for solutions in which each complex is dissolved in an electrochemically stable ionic liquid (*N*-methyl-*N*-propyl-pyrrolidinium TFSA: [P13][TFSA]), as shown in Figure 9.^[52] A current increase, attributed to the oxidation of uncoordinated glymes, was obviously observed at the electrode potential of 4.0 V vs. Li/Li⁺ for the G4/[P13][TFSA] electrolyte. In stark contrast, the anodic limits of the SILs were all higher than 4.5 V vs. Li/Li⁺. The anodic limits, defined at the potential where current density of 20 $\mu\text{A cm}^{-2}$ is observed, were 5.1, 5.0, and 5.3 V vs. Li/Li⁺ for Li, Na, and Mg-SIL electrolytes, respectively, and the order of anodic limits reflects that of ΔHOMO well (Table 3). This observation supports that complexation of glymes with metal ions effectively improves their oxidative stabilities through a HOMO energy level reduction. The substantially high oxidative stability of equimolar complexes also suggests that the uncoordinated glymes scarcely exist in the molten complexes and even in the IL solutions. The magnitude of oxidative stability improvement strongly depends on the coordination center. Metal ions with high charge density in general should impart high stability. As expected, the electrolyte solution with the Li-based SIL showed a higher oxidative stability than that with its Na-based counterpart. Incorporation of Mg^{2+} results in a prominent effect on the oxidative stability improvement, 5.0 V vs. Li/Li⁺ (Figure 9). The strong electric field effect of

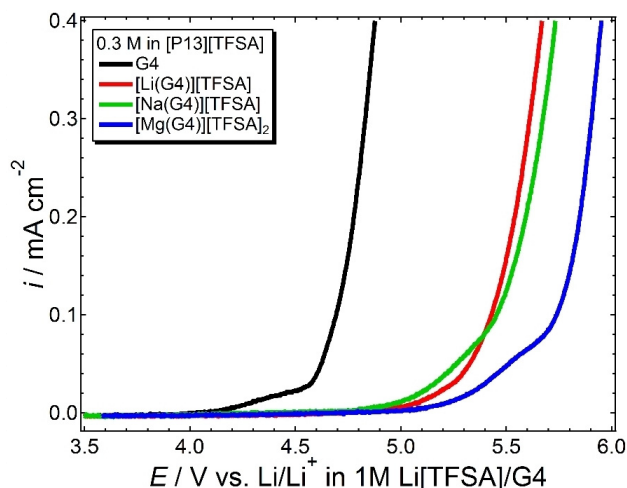


Figure 9. LSV curves of selected equimolar complexes dissolved in [P13][TFSA] measured at 30 °C. Reproduced from Ref. 52 with permission from the American Chemical Society.

small divalent Mg^{2+} ions is the main reason for such a drastic shift in the anodic limit. These remarkable oxidative stabilities allow SILs to be employed as electrolytes with high-voltage positive electrode active materials.

2.3 Possibility as Electrolytes for Na and Mg Batteries

Here, we show examples of battery applications of Na-based SILs. The [Na metal | [Na(G5)][TFSA] | $\text{Na}_{0.44}\text{MnO}_2$ (SMO)] cell showed stable and reversible charge–discharge behavior at 60 °C, as shown in Figure 10a.^[48] This result indicates Na^+ ions are reversibly extracted/inserted from/into the MnO_2 framework. The charge–discharge Coulombic efficiency was approximately 90 % for the initial several cycles and improved up to 95 % for the subsequent cycles. In contrast, the cell

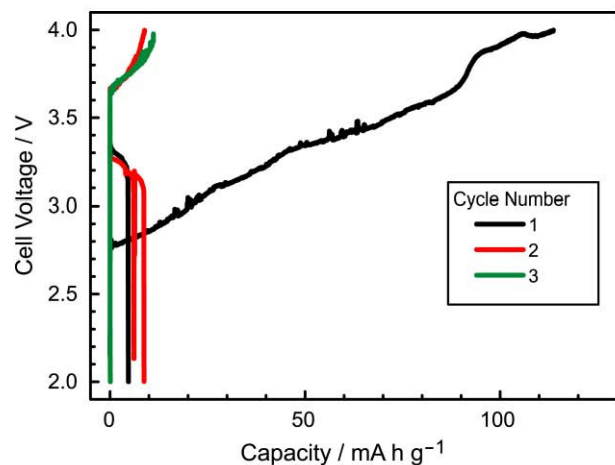
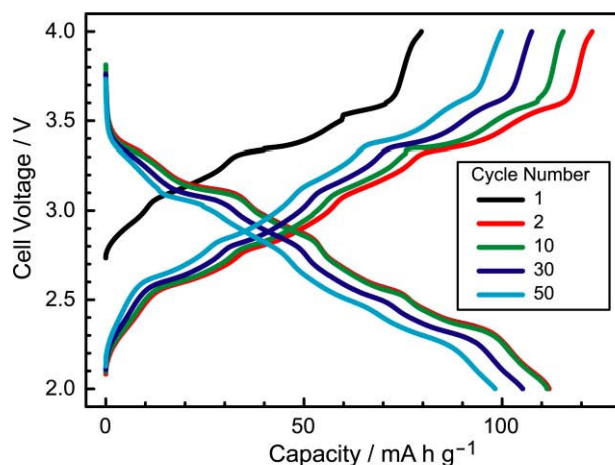


Figure 10. Charge–discharge curves of (upper) [Na|[Na(G5)][TFSA]|SMO] and (lower) [Na|Na[TFSA]/G5 (= 1/1.25)|SMO], operated at 60 °C. Reproduced from Ref. 48 with permission from the PCCP Owner Societies.

incorporating Na[TFSA]/G5 electrolyte solutions, in which excess uncoordinated G5 molecules exist, cannot be cycled (Figure 10b). This poor cycling performance is certainly because of the low oxidative stability of the uncoordinated G5.

Further stable charge–discharge cycling of [Na|SMO] cells can be achieved by using diluted SIL electrolytes. It has been reported that dilution of Li-based SILs using a hydrofluoroether (HFE, $\text{HCF}_2\text{CF}_2\text{OCH}_2\text{CF}_2\text{CF}_2\text{H}$) is significantly effective in improving the transport properties.^[63] In addition, HFE is non-flammable, and one can use HFE-diluted SILs as non-flammable electrolytes for batteries. HFE is also miscible with [Na(glyme)][TFSA], thus making Na-based SILs more favorable for battery applications. The coordination structures of $[\text{Na}(\text{glyme})]^+$ (glyme: G4 or G5) were found to be remain intact in the [Na(glyme)][TFSA]/HFE solutions, strongly suggesting enhanced transport properties of Na-based SILs upon dilution by HFE without losses of their electrochemical stabilities.^[49] The cycling performance of [Na|[Na(glyme)][TFSA]/HFE|SMO] cells were indeed significantly improved compared to those with non-diluted SIL electrolytes. Reversible cycling behavior with stable discharge capacities of ca. 110 mAh g^{-1} was obtained for the cells with [Na(glyme)][TFSA]/HFE for more than 50 cycles. The Coulombic efficiency following the second cycle reached over 99%, suggesting a very minor contribution of undesired side reactions. A mild cycling condition and the high oxidative stability of HFE resulted in this remarkably high Coulombic efficiency,^[43] while the relatively high operation temperature of 60°C for [Na|[Na(G5)][TFSA]|SMO] cells would cause the slight oxidative decomposition of G5, consequently relatively poor Coulombic efficiency. The enhancement in transport properties of SIL electrolytes is also effective in improving the rate capability. As shown in Figure 11, the cell with [Na(G5)][TFSA]/HFE can deliver over 100 mAh g^{-1} even at a 1 C rate (127 mA g^{-1}) at ambient temperature while the cell with the [Na(G5)][TFSA] electrolyte should be cycled at a 1/10 C rate at 60°C to deliver the same level of capacity.

Because of the low solvation ability of HFE, the co-existence of HFE does not disrupt the $[\text{N}(\text{glyme})]^+$ structures but rather facilitates association of $[\text{Na}(\text{glyme})]^+$ and $[\text{TFSA}]^-$. As shown in Figure 12, upon addition of the HFE into [Na(glyme)][TFSA], the association of $[\text{Na}(\text{glyme})]^+$ and $[\text{TFSA}]^-$ is evidenced by the decrease in ionicity, $A_{\text{imp}}/A_{\text{NMR}}$ (A_{imp} is the molar conductivity measured using the complex impedance method and A_{NMR} corresponds to the molar conductivity estimated based on the Nernst-Einstein equation with diffusion coefficients of cations and anions in the electrolytes). The Raman band attributable to the vibrational mode of $[\text{TFSA}]^-$ also clearly reflects a change in cation–anion association state. Note that the ionicity of the G4 system is lower than that of the G5. The binding energy

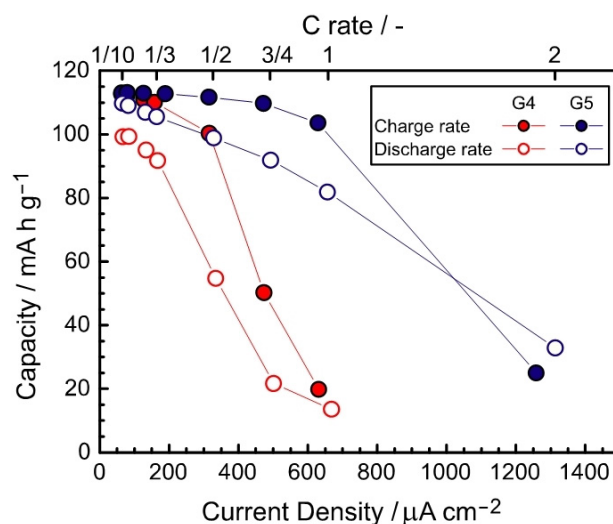


Figure 11. Charge and discharge capacities of [Na|[Na(glyme)][TFSA]/HFE|SMO] cells measured at various current densities. Reproduced from Ref. 49 with permission from the American Chemical Society.

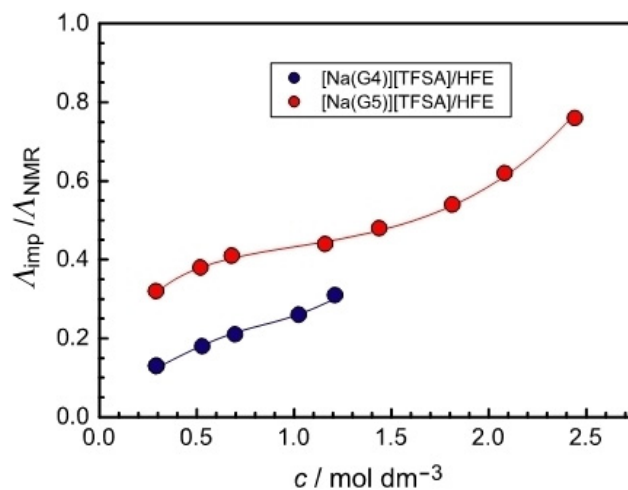


Figure 12. Concentration dependence of ionicity ($A_{\text{imp}}/A_{\text{NMR}}$) for [Na(glyme)][TFSA]/HFE at 30°C . Reproduced from Ref. 49 with permission from the American Chemical Society.

E_{bind} derived from the difference in the stabilization energies (ΔE_{form}) between [Na(glyme)][TFSA] and $[\text{Na}(\text{glyme})]^+$, for [Na(G4)][TFSA] is greater than that for [Na(G5)][TFSA].^[49] The weaker interaction will reduce the lifetime of the ion pair in [Na(G5)][TFSA]/HFE, leading to greater dissociativity (ionicity). The superior rate capability observed for the cell with the [Na(G5)][TFSA]/HFE compared to that with the [Na(G4)][TFSA]/HFE can be explained in part based on ionicity (Figure 11).

The diluted SIL electrolyte, [Na(G5)][TFSA]/HFE, is also compatible with a sulfur cathode. The elemental sulfur

can be electrochemically converted into sodium sulfide, Na_2S , and can theoretically deliver 1672 mAh g^{-1} (10 times larger than conventional intercalation compounds), based on the mass of sulfur loading. Although Na–S batteries have been developed and are already commercialized; those commercialized incorporate solid electrolytes to block dissolution of the sodium polysulfide Na_2S_x ($2 \leq x \leq 8$) into electrolytes and thus require a high operation temperature ($\sim 300^\circ\text{C}$) to achieve sufficient Na^+ ion conductivity. In contrast, Na_2S_x and the related sulfur compounds are hardly soluble in the $[\text{Na}(\text{G5})][\text{TFSA}]/\text{HFE}$ electrolyte owing to its extremely low solvating ability.^[49] Acceptable ionic conductivity of the diluted SIL at ambient temperature allows Na–S batteries to operate at ambient temperature. The Na–S cell incorporating the diluted SIL electrolyte indeed shows a reasonable initial discharge capacity of 975 mAh g^{-1} . Although the capacity faded to ca. 500 mAh g^{-1} within the initial 10 cycles, the cell showed relatively stable charge–discharge behavior during the subsequent cycles (Figure 13).

Replacing $[\text{TFSA}]^-$ by $[\text{FSA}]^-$ (FSA: bis(fluorosulfonyl) amide) is a further effective approach to improve battery performance. The equimolar mixing of $\text{Na}[\text{FSA}]$ and certain glymes also results in stable equimolar complexes $[\text{Na}(\text{glyme})][\text{FSA}]$ (glyme: G4 or G5)^[50] that can be categorized as SILs.^[47] Calculations also strongly support thermally and electrochemically stable solvate formation for $[\text{Na}(\text{G5})][\text{FSA}]$ because of its ΔE_{form} , ΔE_{bind} , and HOMO (or ΔHOMO) energy levels, which are all comparable to those of $[\text{Na}(\text{G5})][\text{TFSA}]$.^[50] The diluted SIL $[\text{Na}(\text{G5})][\text{FSA}]/\text{HFE}$ shows somewhat superior ionic conductivity and viscosity compared to that of $[\text{Na}(\text{G5})][\text{TFSA}]/\text{HFE}$ at the same dilution condition. The difference in the ionic conductivity probably arises mainly from the difference in mobility of the $[\text{FSA}]^-$ and $[\text{TFSA}]^-$ ions.^[24] The $[\text{Na}(\text{G5})][\text{FSA}]/\text{HFE}$ possesses a good oxidative stability, and the SMO cathode can be stably operated in this electrolyte.^[50] The improved transport property of $[\text{Na}(\text{G5})][\text{FSA}]/\text{HFE}$ compared to that of $[\text{Na}(\text{G5})][\text{TFSA}]/\text{HFE}$ affords superior rate capability. The cell with a $[\text{Na}(\text{G5})][\text{FSA}]/\text{HFE}$ electrolyte can deliver 70 mAh g^{-1} even at $1200 \mu\text{A g}^{-1}$, (corresponding to a 2 C rate for SMO), while only 40 mAh g^{-1} can be obtained in $[\text{Na}(\text{G5})][\text{TFSA}]/\text{HFE}$ at the same current density.

The diluted SIL electrolyte $[\text{Na}(\text{G5})][\text{FSA}]/\text{HFE}$ shows remarkable compatibility with various negative/positive electrode materials.^[50] This electrolyte allows reversible deposition/dissolution of Na metals at ambient temperature. The initial Coulombic efficiency was less than 10%; however, the efficiency increased to 95% after 35 cycles (Figure 14), suggesting suppression of irreversible side reactions upon cycling. In stark contrast, reversible Na deposition/dissolution did not occur even after the 2nd cycle in $[\text{Na}(\text{G5})][\text{TFSA}]/\text{HFE}$. This result implies that the $[\text{TFSA}]^-$ ion immediately

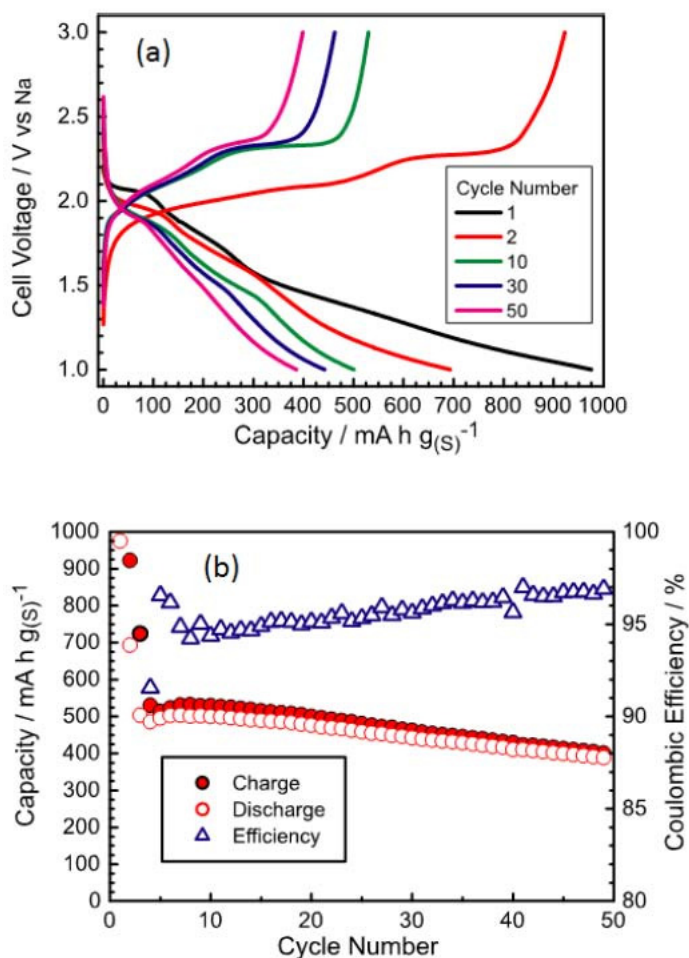


Figure 13. (a) Galvanostatic charge–discharge curves and (b) capacities and Coulombic efficiencies of the $[\text{Na}][\text{Na}(\text{G5})][\text{TFSA}]/\text{HFE}$ (1:4)|S cell measured at a current density of 139 mA g^{-1} , based on the mass of S_8 ($34.8 \mu\text{A cm}^{-2}$) at 30°C . Reproduced from Ref. 49 with permission from the American Chemical Society.

reacts with the deposited Na metal. X-ray photoelectron spectroscopy (XPS) analysis of the Na metal deposited on Cu foil suggested that an effective and thin passivation film containing NaF formed on the Na metal in $[\text{Na}(\text{G5})][\text{FSA}]/\text{HFE}$, resulting in the suppression of electrolyte decomposition.^[50] However, in the case of $[\text{Na}(\text{G5})][\text{TFSA}]/\text{HFE}$, a thicker layer of the decomposition products of the electrolyte formed on the deposited Na metal. This suggests that the layer of decomposition products of $[\text{Na}(\text{G5})][\text{TFSA}]/\text{HFE}$ does not work as an efficient passivation film, and the continuous decomposition of the electrolyte occurs on the Na metal. Thus, the difference in the nature of the passivation film derived from electrolytes significantly affects the Coulombic efficiency of the Na deposition/dissolution.

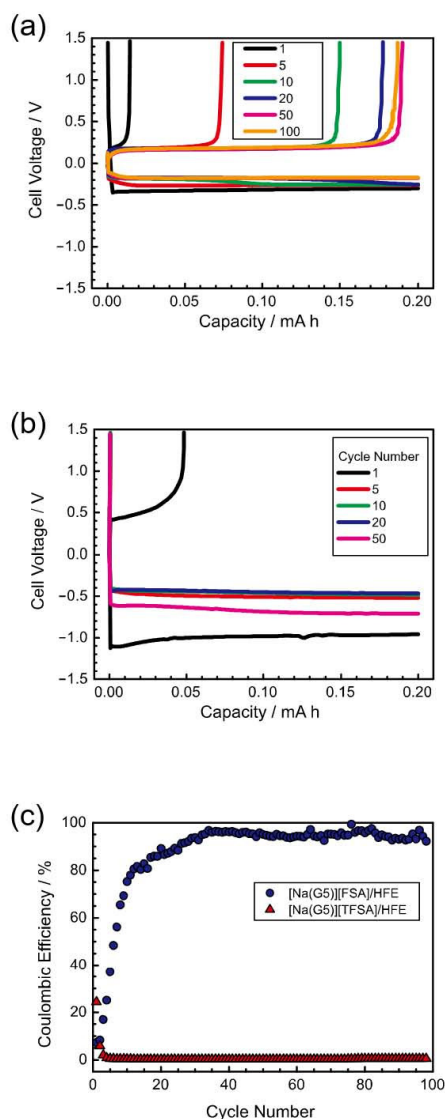


Figure 14. Voltage profile of the deposition and dissolution of the Na metal at a current density of $100 \mu\text{A cm}^{-2}$ in (a) $[\text{Na}][\text{Na}(\text{G5})][\text{FSA}]/\text{HFE}|\text{Cu}$ cell and (b) $[\text{Na}][\text{Na}(\text{G5})][\text{TFSA}]/\text{HFE}|\text{Cu}$ and (c) Coulombic efficiencies for the dissolution/deposition in each cell. Reproduced from Ref. 50 with permission from the American Chemical Society.

Hard carbon (HC) is among the prospective anode materials for Na-ion batteries owing to its remarkable reversibility, acceptable gravimetric/volumetric capacities, and sufficiently low redox voltage.^[64] Various organic solvent and IL-based electrolytes allow reversible Na insertion/extraction into/from parallel graphene layers.^[64–66] The very recent work reported the NaPF_6 -diglyme electrolytes to be one of the fair electrolytes for HC carbon.^[67] The diluted SIL electrolyte $[\text{Na}(\text{G5})][\text{FSA}]/\text{HFE}$ was also found to be compatible with an HC anode, as constant discharge capacities of ca. 240 mAh g^{-1} can be delivered for 300 cycles with a

Coulombic efficiency greater than 99.9% after several cycles (Figure 15). These favorable properties of the $[\text{Na}(\text{G5})][\text{FSA}]/\text{HFE}$ electrolyte promise the development of high energy density Na-ion batteries using Na^+ intercalation compounds for both negative and positive electrodes.

The possibility of Mg-based SILs as electrolytes for high energy density Mg rechargeable batteries was also explored. The $[\text{Mg}(\text{glyme})][\text{TFSA}]_2$ complexes have exceptionally high melting points and are easily crystallized.^[52–54] To reduce the melting temperature of these complexes, an asymmetric homologous of G3 (G3Bu: triethyleneglycol butyl methyl ether) was used as a ligand to suppress crystallization owing to conformational flexibility. This strategy successfully worked to obtain the Mg-based room-temperature SIL $[\text{Mg}(\text{G3Bu})][\text{TFSA}]_2$.^[54] Figure 16 shows the CV and anodic scan of the LSV curves of $[\text{Mg}(\text{G3Bu})][\text{TFSA}]_2$ measured at 60°C . Quasi-reversible electrodeposition/dissolution of the Mg metal was achieved in the electrolyte. The Coulombic efficiency approximately estimated from CV curves is 15%, suggesting that the Mg deposition and the reductive decomposition of $[\text{TFSA}]^-$ simultaneously occurred during the cathodic scan.^[68] Anodic stability, however, reaches up to 4.5 V vs. Li^+/Li . This high stability supports the absence of uncoordinated glymes in the molten $[\text{Mg}(\text{G3Bu})][\text{TFSA}]_2$. The performance of Mg-based SILs is insufficient for practical use at present; however, the design concept of this type of electrolyte will help in realizing high-voltage Mg batteries.

3. Concluding Remarks and Future Perspective

In this account, an overview of a series of SILs consisting of certain glymes and “non-Li” salts was presented with respect to the element strategy. In addition to the Li-based systems, binary mixtures of certain non-Li salts and glymes form stoichiometric complexes. The structural stabilities of the complexes are dominated by the balance of competitive interactions of metal ions with paired anions or glymes, and the structurally stable complexes can also be categorized into SILs. Complexation of glymes with $\text{M}[\text{TFSA}]_n$ salts effectively improves the thermal and electrochemical stabilities. The magnitude of stability enhancement correlates well with the charge density of the metal ions: divalent Mg^{2+} ions impart quite remarkable thermal and electrochemical stabilities compared to monovalent alkali metal ions. Quantum chemical calculations showed the predominant contribution of the electrostatic and induction interactions between the metal ions and glymes to thermal and electrochemical stability enhancement.

Certain Na-based SILs are found to be compatible with various positive and negative electrode materials for Na batteries. Stable charge–discharge cycling with 4 V class

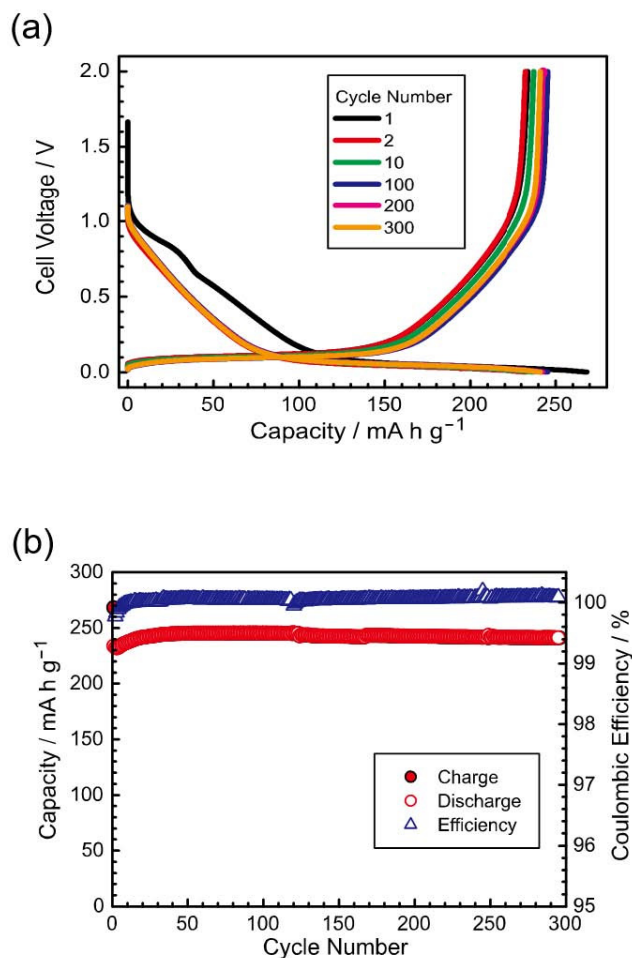


Figure 15. Charge and discharge curves, (b) capacities and Coulombic efficiencies of a $[\text{Na}][\text{Na}(\text{G}5)][\text{FSA}]/\text{HFE}$ (1:4)|HC cell with a current density of 25 mA g^{-1} ($48 \mu\text{A cm}^{-2}$) operated at 30°C . Reproduced from Ref. 50 with permission from the American Chemical Society.

positive electrode material was achieved using Na-based SILs as electrolytes. Dilution of the SILs with HFE and incorporation of $[\text{FSA}]^-$ ions are both effective in improving the battery performance. The $[\text{Na}(\text{G}5)][\text{FSA}]/\text{HFE}$ showed remarkably stable charge–discharge cycling and better rate capability of $[\text{Na}||\text{SMO}$ or HC] cells. Altogether, Na-based SILs are promising electrolytes for next-generation Na-ion batteries. However, the performance of present Na-based SIL electrolytes is still in development for a practical use. Among the issues is the relatively poor reductive stability of the amide-type anions. Replacing them with highly stable and weak Lewis basic anions is a possible approach to address this issue. Novel Na salts, which have attractive properties such as high dissociativity and excellent electrochemical stabilities, have been recently reported.^[69,70] The toxicity of glyme solvents, today G2 and G4 classified as reprotoxic, are also

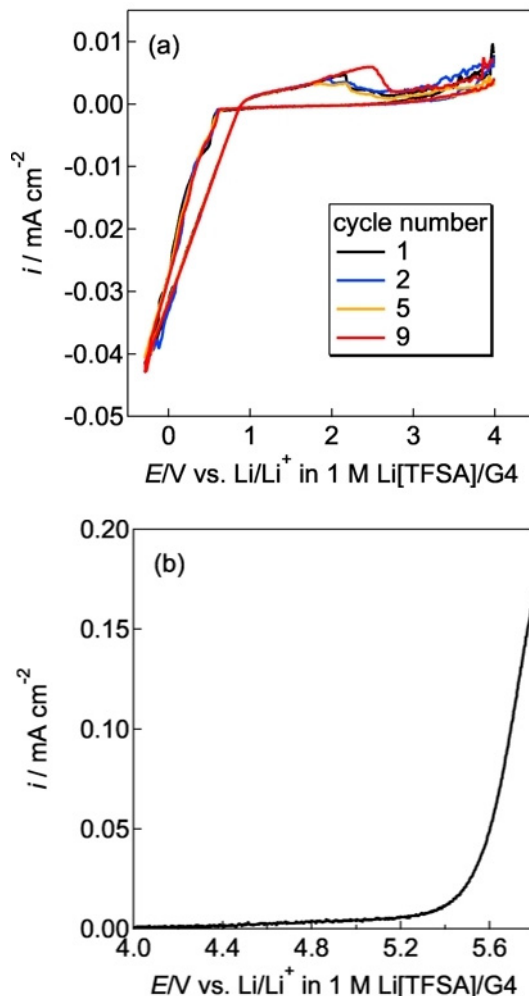


Figure 16. (a) Cyclic voltammograms and (b) anodic scan of a linear sweep voltammogram for $[\text{Mg}(\text{G}3\text{Bu})][\text{TfSA}]_2$ at 60°C , with scan rates of 1 mV s^{-1} . Reproduced from Ref. 54 with permission from the PCCP Owner Societies.

problematic for practical applications.^[71,72] The use of different ligands seems effective in improving both the stability and safety of electrolytes.^[73] A combination of such new materials and our concept of electrolyte design may open the possibility to create electrolytes for practical Na batteries.

K-based batteries are promising post Li-ion batteries owing to some advantageous electrochemical properties compared to its Li- and Na-based counterparts.^[6,7] K-based SIL electrolytes are a possible candidate to achieve K-based batteries without a safety concern of electrolytes.^[51] In addition, the concept itself is particularly promising with regards to achieving multivalent metal-based batteries, as such batteries should be cycled at higher temperatures to deliver reasonable capacities.^[74–76] Multivalent metal-based molten complexes, which are electrochemically active, have been

reported elsewhere.^[77–79] These molten complexes are promising electrolytes for multivalent metal-based batteries.

Taken altogether, favorable thermal and electrochemical stabilities of SIL-based electrolytes are expected to contribute to the thermal stability of next generation batteries. However, for practical use of SILs in batteries, further examinations, such as detailed studies on toxicity, corrosiveness, and ignitability of SILs, and thermal runaway test of batteries with SILs, are required.

Acknowledgements

The authors acknowledge Dr. Seiji Tsuzuki (National Institute of Advanced Industrial Science and Technology) for collaboration in the quantum chemical calculations, and Prof. Yasuhiro Umebayashi (Niigata University) for his kind advice on Raman spectroscopic study. This study was supported in part by the MEXT program “Elements Strategy Initiative to Form Core Research Center” of the Ministry of Education, Culture, Sports, Science, and Technology (MEXT) of Japan, the JSPS KAKENHI (Grant Nos. 16H06368 and 18H03926) from the Japan Society for the Promotion of Science (JSPS), and the ALCA-SPRING Project from the Japan Science and Technology Agency (JST).

References

- [1] N. Yabuuchi, M. Kajiyama, J. Iwatate, H. Nishikawa, S. Hitomi, R. Okuyama, R. Usui, Y. Yamada, S. Komaba, *Nat. Mater.* **2012**, *11*, 512–517.
- [2] N. Yabuuchi, K. Kubota, M. Dahbi, S. Komaba, *Chem. Rev.* **2014**, *114*, 11636–11682.
- [3] J.-Y. Hwang, S.-T. Myung, Y.-K. Sun, *Chem. Soc. Rev.* **2017**, *46*, 3529–3614.
- [4] P. K. Nayak, L. Yang, W. Brehm, P. Adelhelm, *Angew. Chem. Int. Ed.* **2018**, *57*, 102–120; *Angew. Chem.* **2018**, *130*, 106–126.
- [5] S. Wei, S. Xu, A. Agrawal, S. Choudhury, Y. Lu, Z. Tu, L. Ma, L. A. Archer, *Nat. Commun.* **2016**, *7*, 11722.
- [6] K. Kubota, M. Dahbi, T. Hosaka, S. Kumakura, S. Komaba, *Chem. Rec.* **2018**, *18*, 459–479.
- [7] S. Komaba, T. Hasegawa, M. Dahbi, K. Kubota, *Electrochem. Commun.* **2015**, *60*, 172–175.
- [8] C. Vaalma, D. Buchholz, S. Passerini, *Curr. Opin. Electrochem.* **2018**, in press, doi: 10.1016/j.coelec.2018.03.031.
- [9] J. Muldoon, C. B. Bucur, T. Gregory, *Chem. Rev.* **2014**, *114*, 11683–11720.
- [10] D. Aurbach, Z. Lu, A. Shechter, Y. Gofer, H. Gizbar, R. Turgeman, Y. Cohen, M. Moshkovich, E. Levi, *Nature* **2000**, *407*, 724–727.
- [11] Z. Z. -Karger, X. Zhao, D. Wang, T. Diemant, R. J. Behm, M. Fichtner, *Adv. Energy Mater.* **2014**, 1401155.
- [12] A. Ponrouch, C. Frontera, F. Barde, M. R. Palacin, *Nat. Mater.* **2016**, *15*, 169–172.
- [13] D. Wang, X. Gao, Y. Chen, L. Jin, C. Kuss, P. G. Bruce, *Nat. Mater.* **2018**, *17*, 16–20.
- [14] M.-C. Lin, M. Gong, B. Lu, Y. Wu, D.-Y. Wang, M. Guan, M. Angell, C. Chem, J. Yang, B.-J. Hwang, H. Dai, *Nature* **2015**, *520*, 324–328.
- [15] M. Angell, C.-J. Pan, Y. Rong, C. Yuan, M.-C. Lin, B.-J. Hwang, H. Dai, *Proc. Natl. Acad. Sci. India* **2017**, *113*, 834–839.
- [16] T. Mandai, P. Johansson, *J. Mater. Chem. A* **2015**, *3*, 12230–12239.
- [17] G. A. Giffin, *J. Mater. Chem. A* **2016**, *4*, 13378–13389.
- [18] M. Watanabe, M. L. Thomas, S. Zhang, K. Ueno, T. Yasuda, K. Dokko, *Chem. Rev.* **2017**, *117*, 7190–7239.
- [19] C. A. Angell, Y. Ansari, Z. F. Zhao, *Faraday Discuss.* **2012**, *154*, 9–27.
- [20] T. Mandai, K. Yoshida, K. Ueno, K. Dokko, M. Watanabe, *Phys. Chem. Chem. Phys.* **2014**, *16*, 8761–8772.
- [21] T. Tamura, K. Yoshida, T. Hachida, M. Tsuchiya, M. Nakamura, Y. Kazue, N. Tachikawa, K. Dokko, M. Watanabe, *Chem. Lett.* **2010**, *39*, 753–755.
- [22] K. Yoshida, M. Tsuchiya, N. Tachikawa, K. Dokko, M. Watanabe, *J. Phys. Chem. C* **2011**, *115*, 18384–18394.
- [23] K. Yoshida, M. Nakamura, Y. Kazue, N. Tachikawa, S. Tsuzuki, S. Seki, K. Dokko, M. Watanabe, *J. Am. Chem. Soc.* **2011**, *113*, 13121–13129.
- [24] K. Ueno, K. Yoshida, M. Tsuchiya, N. Tachikawa, K. Dokko, M. Watanabe, *J. Phys. Chem. B* **2012**, *116*, 11323–11331.
- [25] C. Zhang, K. Ueno, A. Yamazaki, K. Yoshida, H. Moon, T. Mandai, Y. Umebayashi, K. Dokko, M. Watanabe, *J. Phys. Chem. B* **2014**, *118*, 5144–5153.
- [26] S. Tsuzuki, W. Shinoda, M. Matsugami, Y. Umebayashi, K. Ueno, T. Mandai, S. Seki, K. Dokko, M. Watanabe, *Phys. Chem. Chem. Phys.* **2015**, *17*, 126–129.
- [27] K. Ueno, R. Tatara, S. Tsuzuki, S. Saito, H. Doi, K. Yoshida, T. Mandai, M. Matsugami, Y. Umebayashi, K. Dokko, M. Watanabe, *Phys. Chem. Chem. Phys.* **2015**, *17*, 8248–8257.
- [28] T. Mandai, K. Yoshida, S. Tsuzuki, R. Nozawa, H. Masu, K. Ueno, K. Dokko, M. Watanabe, *J. Phys. Chem. B* **2015**, *119*, 1523–1534.
- [29] M. Watanabe, K. Dokko, K. Ueno, M. L. Thomas, *Bull. Chem. Soc. Jpn.* **2018**, accepted. doi: 10.1246/bcsj.20180216.
- [30] Y. Choquette, G. Brisard, M. Parent, D. Brouillette, G. Perron, J. E. Desnoyers, M. Armand, D. Gravel, N. Slougi, *J. Electrochem. Soc.* **1998**, *145*, 3500–3507.
- [31] D. Brouillette, D. E. Irish, N. J. Taylor, G. Perron, M. Odziemkowski, J. E. Desnoyers, *Phys. Chem. Chem. Phys.* **2002**, *4*, 6063–6071.
- [32] W. A. Henderson, F. McKenna, M. A. Khan, N. R. Brooks, V. G. Young Jr., R. Frech, *Chem. Mater.* **2005**, *17*, 2284–2289.
- [33] W. A. Henderson, N. R. Brooks, W. W. Brennessel, V. G. Young Jr., *Chem. Mater.* **2003**, *15*, 4679–4684.
- [34] W. A. Henderson, N. R. Brooks, V. G. Young Jr., R. Frech, *Chem. Mater.* **2003**, *15*, 4685–4690.
- [35] T. M. Papperfus, W. A. Henderson, B. B. Owns, K. R. Mann, W. H. Smyrl, *J. Electrochem. Soc.* **2004**, *151*, A209–A215.

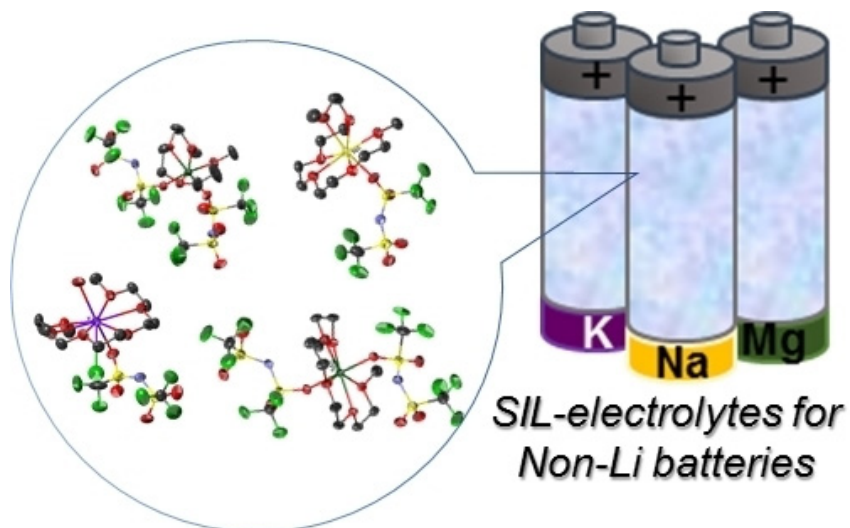
- [36] J. Grondin, J.-L. Lassègues, M. Chami, L. Servant, D. Talaga, W. A. Henderson, *Phys. Chem. Chem. Phys.* **2004**, *6*, 4260–4267.
- [37] A. Dolan, D. A. Sherman, R. Atkin, G. G. Warr, *ChemPhysChem* **2016**, *17*, 3096–3101.
- [38] P. Jankowski, M. Dranka, G. Z. Żukowska, J. Zachara, *J. Phys. Chem. C* **2015**, *119*, 9108–9116.
- [39] P. Jankowski, M. Dranka, G. Z. Żukowska, *J. Phys. Chem. C* **2015**, *119*, 10247–10254.
- [40] G. Vanhoutte, N. R. Brooks, S. Schaltin, B. Opperdoes, L. V. Meervelt, J.-P. Locquet, P. M. Vereecken, J. Fransaer, K. Binnemans, *J. Phys. Chem. C* **2014**, *118*, 20152–20162.
- [41] S. Tsuzuki, W. Shinoda, S. Seki, Y. Umebayashi, K. Yoshida, K. Dokko, M. Watanabe, *ChemPhysChem* **2013**, *14*, 1993–2001.
- [42] K. Ueno, J.-W. Park, A. Yamazaki, T. Mandai, N. Tachikawa, K. Dokko, M. Watanabe, *J. Phys. Chem. C* **2013**, *117*, 20509–20516.
- [43] H. Moon, T. Mandai, R. Tatara, K. Ueno, A. Yamazaki, K. Yoshida, S. Seki, K. Dokko, M. Watanabe, *J. Phys. Chem. C* **2015**, *119*, 3957–3970.
- [44] K. Ikeda, S. Terada, T. Mandai, K. Ueno, K. Dokko, M. Watanabe, *Electrochemistry* **2015**, *83*, 914–917.
- [45] H.-M. Kwon, M. L. Thomas, R. Tatara, A. Nakanishi, K. Dokko, M. Watanabe, *Chem. Lett.* **2017**, *46*, 573–576.
- [46] H.-M. Kwon, M. L. Thomas, R. Tatara, Y. Oda, Y. Kobayashi, A. Nakanishi, K. Ueno, K. Dokko, M. Watanabe, *ACS Appl. Mater. Interfaces* **2017**, *9*, 6014–6021.
- [47] T. Mandai, R. Nozawa, S. Tsuzuki, K. Yoshida, K. Ueno, K. Dokko, M. Watanabe, *J. Phys. Chem. B* **2013**, *117*, 15072–15085.
- [48] S. Terada, T. Mandai, R. Nozawa, K. Yoshida, K. Ueno, S. Tsuzuki, K. Dokko, M. Watanabe, *Phys. Chem. Chem. Phys.* **2014**, *16*, 11737–11746.
- [49] S. Terada, H. Susa, S. Tsuzuki, T. Mandai, K. Ueno, Y. Umebayashi, K. Dokko, M. Watanabe, *J. Phys. Chem. C* **2016**, *120*, 23339–23350.
- [50] S. Terada, H. Susa, S. Tsuzuki, T. Mandai, K. Ueno, K. Dokko, M. Watanabe, *J. Phys. Chem. C*, **2018**, *122*, 16589–16599.
- [51] T. Mandai, S. Tsuzuki, K. Ueno, K. Dokko, M. Watanabe, *Phys. Chem. Chem. Phys.* **2015**, *17*, 2838–2849.
- [52] S. Terada, T. Mandai, S. Suzuki, S. Tsuzuki, K. Watanabe, Y. Kamei, K. Ueno, K. Dokko, M. Watanabe, *J. Phys. Chem. C* **2016**, *120*, 1353–1365.
- [53] S. Tsuzuki, T. Mandai, S. Suzuki, W. Shinoda, T. Nakamura, T. Morishita, K. Ueno, S. Seki, Y. Umebayashi, K. Dokko, M. Watanabe, *Phys. Chem. Chem. Phys.* **2017**, *19*, 18262–18272.
- [54] K. Hashimoto, S. Suzuki, M. L. Thomas, T. Mandai, S. Tsuzuki, K. Dokko, M. Watanabe, *Phys. Chem. Chem. Phys.* **2018**, *20*, 7998–8007.
- [55] W. Huang, R. Frech, P. Johansson, J. Lindgren, *Electrochim. Acta* **1995**, *40*, 2147–2151.
- [56] P. Geysens, V. S. Rangasamy, S. Thayumanasundaram, K. Robeyns, L. V. Meervelt, J.-P. Locquet, J. Fransaer, K. Binnemans, *J. Phys. Chem. B* **2018**, *122*, 275–289.
- [57] T. Mandai, H. Masu, P. Johansson, *Dalton Trans.* **2015**, *44*, 11259–11263.
- [58] C. Zhang, D. Ainsworth, Y. G. Andreev, P. G. Bruce, *J. Am. Chem. Soc.* **2007**, *129*, 8700–8701.
- [59] C. P. Rhodes, R. Frech, *Macromolecules* **2001**, *34*, 2660–2666.
- [60] P. Johansson, J. Grondin, J.-C. Lassègues, *J. Phys. Chem. A* **2010**, *114*, 10700–10705.
- [61] P. Jankowski, M. Dranka, W. Wiczorek, P. Johansson, *J. Phys. Chem. Lett.* **2017**, *8*, 3678–3682.
- [62] M. Hayyan, F. S. Mjalli, M. A. Hashim, I. M. AlNashef, T. X. Mei, *J. Ind. Eng. Chem.* **2013**, *19*, 106–112.
- [63] K. Dokko, N. Tachikawa, K. Yamauchi, M. Tsuchiya, A. Yamazaki, E. Takashima, J.-W. Park, K. Ueno, S. Seki, N. Serizawa, M. Watanabe, *J. Electrochem. Soc.* **2013**, *160*, A1304–A1310.
- [64] S. Komaba, W. Murata, T. Ishikawa, N. Yabuuchi, T. Ozeki, T. Nakayama, A. Ogata, K. Gotoh, K. Fujiwara, *Adv. Funct. Mater.* **2011**, *21*, 3859–3867.
- [65] A. Ponrouch, A. R. Goni, M. R. Palacin, *Electrochem. Commun.* **2013**, *27*, 85–88.
- [66] C. Ding, T. Nohira, R. Hagiwara, A. Fukunaga, S. Sakai, K. Nitta, *Electrochim. Acta* **2015**, *176*, 344–349.
- [67] K. Westman, R. Dugas, P. Jankowski, W. Wiczorek, G. Gachot, M. Morcrette, E. Irisarri, A. Pourouch, M. R. Palacin, J.-M. Tarascon, P. Johansson, *Appl. Energy* **2018**, *1*, 2671–2680.
- [68] N. N. Rajput, X. Qu, N. Sa, A. K. Burrell, K. A. Persson, *J. Am. Chem. Soc.* **2015**, *137*, 3411–3420.
- [69] S. Bulut, P. Klose, I. Krossing, *Dalton Trans.* **2011**, *40*, 8114–8124.
- [70] A. P. -Marczewska, T. Trzeciak, A. Bitner, L. Niedzicki, M. Dranka, G. Z. Żukowska, M. Marcinek, W. Wiczorek, *Chem. Mater.* **2014**, *26*, 4908–4914.
- [71] M. M. Archuleta, *J. Power Sources* **1995**, *54*, 138–142.
- [72] P. Yoganantharajar, D. J. Eyckens, J. L. Pedrina, L. C. Henderson, W. Gibert, *New J. Chem.* **2016**, *40*, 6559–6603.
- [73] K. Takada, Y. Yamada, E. Watanabe, J. Wang, K. Sodeyama, Y. Tateyama, K. Hirata, T. Kawase, A. Yamada, *ACS Appl. Mater. Interfaces* **2017**, *9*, 33802–33809.
- [74] M. Liu, Z. Rong, R. Malik, P. Canepa, A. Jain, G. Ceder, K. A. Persson, *Energy Environ. Sci.* **2015**, *8*, 964–974.
- [75] V. Duffort, X. Sun, L. F. Nazar, *Chem. Commun.* **2016**, *52*, 12458–12461.
- [76] T. Mandai, Y. Akita, S. Yagi, M. Egashira, H. Munakata, K. Kanamura, *J. Mater. Chem. A*, **2017**, *5*, 3152–3156.
- [77] M. Steichen, N. R. Brooks, L. V. Meervelt, J. Fransaer, K. Binnemans, *Dalton Trans.* **2014**, *43*, 12329–12341.
- [78] S. Schaltin, N. R. Brooks, J. Sniekers, L. V. Meervelt, K. Binnemans, J. Fransaer, *Chem. Commun.* **2014**, *50*, 10248–10250.
- [79] T. Mandai, P. Johansson, *J. Phys. Chem. C* **2016**, *120*, 21285–21292.

Received: July 27, 2018

Accepted: September 14, 2018

Published online on ■■■ ■■■ ■■■ ■■■ ■■■

PERSONAL ACCOUNT



T. Mandai, K. Dokko, M. Watanabe*

1 – 16

Solvate Ionic Liquids for Li, Na, K, and Mg Batteries

Solvate ionic liquids particularly those incorporating cost-effective earth-abundant non-Li metal ions such as Na^+ , K^+ , and Mg^{2+} , are promising electrolytes to realize safe and highly efficient large-scale electrochemical energy storage systems. In this account, the fundamental aspects and characteristics for electrolyte applications of SILs consisting of glymes and

non-Li salts are reported. The balance of competitive interactions of anions and ligands with metal ions was found to predominate the stability of the solvate cations. Suitable combinations of salts, ligands, and diluents resulted in electrolytes showing excellent stability and remarkable battery performance.
